Journal of Colloid and Interface Science 357 (2011) 521–526

Contents lists available at ScienceDirect

Journal of Colloid and Interface Science

www.elsevier.com/locate/jcis

On steady two-fluid electroosmotic flow with full interfacial electrostatics

WooSeok Choi [a,b], Ashutosh Sharma [c,d], Shizhi Qian [c,e], Geunbae Lim [a,b], Sang Woo Joo [c,*]

[a] Department of Mechanical Engineering, Postech, Pohang 790-784, Republic of Korea
[b] Division of Integrative Bioscience and Biotechnology, Postech, Pohang 790-784, Republic of Korea
[c] School of Mechanical Engineering, Yeungnam University, Gyongsan 705-030, Republic of Korea
[d] Department of Chemical Engineering, Indian Institute of Technology, Kanpur 208016, India
[e] Department of Aerospace Engineering, Old Dominon University, Norfolk, VA 23529, USA

ARTICLE INFO

Article history:
Received 16 November 2010
Accepted 31 January 2011

Keywords:
Electroosmosis
Interface
Maxwell stress
Two-fluid

ABSTRACT

A two-fluid electroosmotic flow in a microchannel is studied by considering full hydrodynamic and electrostatic interactions on the interface. Jumps in electrical potential and in charge density across the interface, in particular, are found to create counterintuitive flow behavior through the electrostatic interaction of the interface with the external field imposed. The interfacial electrostatic effects are shown to induce flow reversal within physically reasonable parametric ranges. It is also shown that the electrostatic properties of the interface must be carefully considered in electroosmotic pumping lest the nonconducting fluid should stay stationary or flow in an unintended direction. A formula for quantitative control of electroosmotic pumping is provided.

1. Introduction

Electroosmosis is one of the most common techniques for controlling liquid motions in a microfluidic system, where pressure-driven flows are usually inefficient, despite its potential problems, such as electrolysis of water, electrochemical decomposition of the solute, generation of gases, and fluctuation of pH. It is, however, not effective with nonconducting or weakly conducting fluids, such as oils and organic solvents. To drive such fluids by electroosmosis, a two-layer system is proposed, where a fluid layer with high electroosmotic mobility drags another layer through the shear stress at the interface between the two fluid layers [1,2].

It is important to understand in detail the dynamics of two-fluid electroosmotic flows by properly modeling contributions of the hydrodynamic and electrostatic stress components at the interface, among other parts of the flow. At the interface of two immiscible electrolyte solutions, a narrow region exists where the electric potential changes abruptly due to the adsorption of ions [3,4]. The sharp change at this Helmholtz layer can often be described by a zeta-potential jump across the interface. Fluid motions induced by the Maxwell stress associated with these ions can be explained by the Taylor–Melcher theory, as described in detail by Melcher and Taylor [5], Saville [6], and Burcham and Saville [7]. Theoretical studies on droplet deformation by Silver et al. [8] and Supeene et al. [9] and on interfacial instabilities of thin fluid films by Verma et al. [10] and Shankar and Sharma [11] show the importance of the Maxwell stress on interfaces. Choi et al. [12] recently report interesting counterintuitive fluid motions induced by this interfacial Maxwell stress in the electroosmotic flow of a single layer bounded above by an inert gas.

Gao et al. [13] and Ngoma and Erchiqui [14] analyzed steady two-layer electroosmotic flows in a rectangular microchannel and between two parallel plates (two-dimensional flow but with simultaneous streamwise pressure gradient), respectively, by assuming a Poisson–Boltzmann distribution of ions and further applying the Debye–Hückel approximation. Across the interface the shear stress is taken to be continuous, which should be appropriate if no electrostatic contribution were present at the interface. Gao et al. [15] make a proper amendment to this problem by incorporating the Maxwell stress at the interface for transient two-layer electroosmotic flows. Gao et al. [16] further consider the effect of simultaneous pressure gradients. A coaxial two-fluid electroosmotic flow in a circular microchannel is analyzed similarly by Liu et al. [17].

Although some basic features of two-fluid electroosmosis are reported in the aforementioned studies, much of its rich nature remains to be examined, including that related to the flow reversal due to interface electrostatics [12], through a careful parametric study. In the present study, we achieve this goal by considering a two-dimensional two-fluid electroosmotic flow between parallel plates, without complications with benign side walls. Instead of taking one of the layers to be nonconductive, as in the previous studies, we analyze the hydrodynamic and electrostatic responses of both layers by taking arbitrary permittivity.

* Corresponding author.
E-mail address: swjoo@yu.ac.kr (S.W. Joo).

0021-9797/$ - see front matter © 2011 Elsevier Inc. All rights reserved.
doi:10.1016/j.jcis.2011.01.107

2. Mathematical formulation

We consider a steady unidirectional electroosmotic flow of two immiscible viscous fluids of constant density ρ_i, kinematic viscosity ν_i, electric permittivity ϵ_i, and thickness d_i confined between two parallel planes at distance d ($=d_1+d_2$), as shown in Fig. 1, where $i=1$ and 2 are associated with the upper (fluid 1) and the lower layer (fluid 2), respectively. The flow is generated by the electrostatic reaction between a constant imposed direct-current electric field E_{el} and excess ions in the electric double layers (EDLs) adjacent to the top ($i=1$) and bottom ($i=2$) planes, characterized by the Debye length λ_{Di} and the zeta potential ζ_i ($i=1$ and 2), and by viscous dissipation outside the EDLs.

We nondimensionalize the system by using d and $E_{el}d$ as unit length and electrical potential, respectively, and write the total electric potential in each fluid as $\phi_i(x,y) = -x + \varphi_i(y)$, where $-x$ and $\varphi_i(y)$ represent, respectively, electrical potential due to external electric field applied and zeta potential in a Cartesian coordinate system, as shown in Fig. 1. If we limit the present analysis to microchannels, where the Debye lengths are much smaller than the channel thickness d, the electric potential φ_i due to the zeta potential can be described by the Poisson–Boltzmann equation, which is linearized using the Debye–Hückel approximation as

$$\nabla^2\varphi_i = \frac{\varphi_i}{\mathrm{De}_i^2}, \tag{1}$$

where $\mathrm{De}_i = \lambda_{Di}/d$ is the nondimensional Debye length.

Dimensionless boundary conditions for the potential then are $\varphi_1 = Z_1$ at $y = h_1$ and $\varphi_2 = Z_2$ at $y = -h_2$, where the nondimensional zeta potential $Z_i = \zeta_i/(E_{el}d)$ and the layer thickness $h_i = d_i/d$. At the interface between two fluids ($y=0$), two boundary conditions are required. Here we impose the zeta potential difference ($\Delta\zeta$) and Gauss's law for the electrical displacement,

$$\varphi_1 - \varphi_2 = Z_D \tag{2}$$

$$\frac{\partial\phi_1}{\partial y} - \epsilon_r\frac{\partial\phi_2}{\partial y} = -Q, \tag{3}$$

where $Z_D = \Delta\zeta/(E_{el}d)$ is the dimensionless potential difference at the interface, $\epsilon_r = \epsilon_2/\epsilon_1$ is the permittivity ratio, and $Q = q_s/(\epsilon_1 E_{el})$ is the dimensionless surface charge density. Here Z_D and Q are considered to be independent parameters. Samec et al. [18] studied double layers at the interface between two immiscible electrolyte solutions, and showed that for a given potential difference across the interface the surface charge densities can be varied depending on the salt concentrations.

The solutions to the Poisson–Boltzmann equation subjected to the above boundary conditions are obtained as

$$\varphi_1 = Z_1\left[f_1\cosh\frac{y}{\mathrm{De}_1} + \frac{1-f_1\cosh(h_1/\mathrm{De}_1)}{\sinh(h_1/\mathrm{De}_1)}\sinh\frac{y}{\mathrm{De}_1}\right] \quad (0\le y\le h_1) \tag{4}$$

$$\varphi_2 = Z_2\left[f_2\cosh\frac{y}{\mathrm{De}_2} - \frac{1-f_2\cosh(h_2/\mathrm{De}_2)}{\sinh(h_2/\mathrm{De}_2)}\sinh\frac{y}{\mathrm{De}_2}\right] \quad (-h_2\le y\le 0), \tag{5}$$

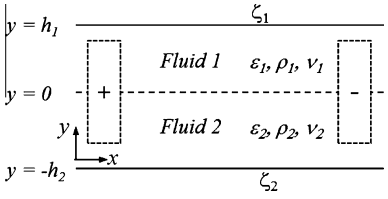

Fig. 1. Schematic diagram of two-layer electroosmotic system.

where

$$f_1 = \frac{\left[\mathrm{csch}\frac{h_1}{\mathrm{De}_1} + \frac{\epsilon_r}{\mathrm{De}_r}\left(Z_R\mathrm{csch}\frac{h_2}{\mathrm{De}_2} + Z_D\coth\frac{h_2}{\mathrm{De}_2}\right)\right] + \frac{Q\cdot\mathrm{De}_1}{Z_1}}{\coth\frac{h_1}{\mathrm{De}_1} + \frac{\epsilon_r}{\mathrm{De}_r}\coth\frac{h_2}{\mathrm{De}_2}}, \tag{6}$$

$$f_2 = \frac{\left[\frac{1}{Z_R}\mathrm{csch}\frac{h_1}{\mathrm{De}_1} - \frac{Z_D}{Z_R}\coth\frac{h_1}{\mathrm{De}_1} + \frac{\epsilon_r}{\mathrm{De}_r}\mathrm{csch}\frac{h_2}{\mathrm{De}_2}\right] + \frac{Q\cdot\mathrm{De}_1}{Z_2}}{\coth\frac{h_1}{\mathrm{De}_1} + \frac{\epsilon_r}{\mathrm{De}_r}\coth\frac{h_2}{\mathrm{De}_2}} \tag{7}$$

Here the zeta potential ratio $Z_R = \zeta_2/\zeta_1$, and the Debye length ratio $\mathrm{De}_r = \mathrm{De}_2/\mathrm{De}_1$.

For steady unidirectional flow the x-component of the conservation of momentum for each fluid is expressed as

$$0 = \frac{\partial^2 u_1}{\partial y^2} - \frac{E_{O1}}{Z_1}\nabla^2\phi_1, \tag{8}$$

$$0 = \frac{\partial^2 u_2}{\partial y^2} - \nu_r\frac{E_{O2}}{Z_2}\nabla^2\phi_2, \tag{9}$$

where the ratio of kinematic viscosities $\nu_r = \nu_2/\nu_1$. Here the electroosmotic number for each fluid, $E_{Oi} = (\epsilon_i E_{el} d\zeta_i)/(\rho_i\nu_i^2)$, measures the driving force in each layer, and is proportional to the electrical field imposed and the surface zeta potential. Using Eqs. (4) and (5), we get

$$0 = \frac{\partial^2 u_1}{\partial y^2} - \frac{E_{O1}}{Z_1\mathrm{De}_1^2}\varphi_1, \tag{10}$$

$$0 = \frac{\partial^2 u_2}{\partial y^2} - \nu_r\frac{E_{O2}}{Z_2\mathrm{De}_2^2}\varphi_2. \tag{11}$$

On the top and bottom planes no-slip boundary conditions $u_1 = 0$ at $y = h_1$ and $u_2 = 0$ at $y = -h_2$ are to be imposed. On the interface ($y=0$), the streamwise component of the velocity vector and the surface traction must be continuous:

$$u_1 = u_2, \tag{12}$$

$$\frac{\partial u_1}{\partial y} - \frac{E_{O1}}{Z_1}\frac{\partial\varphi_1}{\partial y} = \mu_r\left(\frac{\partial u_2}{\partial y} - \nu_r\frac{E_{O2}}{Z_2}\frac{\partial\varphi_2}{\partial y}\right). \tag{13}$$

The above system yields the x-component velocity vector u_i for each layer as

$$u_1 = E_{O1}\left[f_1\cosh\frac{y}{\mathrm{De}_1} + \frac{1-f_1\cosh(h_1/\mathrm{De}_1)}{\sinh(h_1/\mathrm{De}_1)}\sinh\frac{y}{\mathrm{De}_2} - \frac{\mu_r}{\mu_r h_1 + h_2}\left\{1 - \nu_r\frac{E_{O2}}{E_{O1}} - \left(f_1 - \nu_r\frac{E_{O2}}{E_{O1}}f_2\right)\right\}(y-h_1) - 1\right], \tag{14}$$

$$u_2 = \nu_r E_{O2}\left[f_2\cosh\frac{y}{\mathrm{De}_2} + \frac{1-f_2\cosh(h_2/\mathrm{De}_2)}{\sinh(h_2/\mathrm{De}_2)}\sinh\frac{y}{\mathrm{De}_2} - \frac{1}{\mu_r h_1 + h_2}\left\{1 - \frac{E_{O1}}{\nu_r E_{O2}} - \left(\frac{E_{O1}}{\nu_r E_{O2}}f_1 - f_2\right)\right\}(y+h_2) - 1\right], \tag{15}$$

where μ_r is the ratio of dynamic viscosities. From these the interfacial velocity is easily obtained as

$$u(0) = -\{E_{O1}h_2(1-f_1) + E_{O2}h_1(1-f_2)\}/(\mu_r h_1 + h_2). \tag{16}$$

3. Discussion

Unidirectional velocity profiles for two-fluid electroosmotic flow in a microchannel can be studied by imposing physically realistic sets of parameters on Eqs. (14) and (15). Among numerous sets tried, we present here only results of great consequence. For two conducting fluids, we focus on a parametric study for the viscosity ratio μ_r, permittivity ratio ϵ_r, interfacial potential jump Z_D, and interfacial charge-density jump $-Q$ while keeping the channel width fixed in microscale ($\mathrm{De}_1 = \mathrm{De}_2 = 0.05$). The thickness of fluids equal ($h_1 = h_2 = 1/2$), and the zeta potentials on the channel wall identical ($Z_R = 1$). The electroosmotic numbers E_{Oi}'s

can be scaled out, as seen below. We then discuss the effect of different Debye lengths of each layer, and in particular a case in which one of the fluids is nonconducting (infinite Debye length) and dragged by shear stress on the interface.

Fig. 2 shows velocity profiles when neither the jump in interfacial potential nor that in interfacial charge is present ($Z_D = 0$ and $Q = 0$). In Fig. 2a, the viscosities of the two fluids are different, whereas in Fig. 2b the permittivities are different. As can easily be understood, the maximum velocity occurs in the fluid with lower viscosity in Fig. 2a. The profile for equal viscosity ($\mu_r = 1$) represents a typical single-fluid electroosmotic flow in a microchannel. The interfacial velocity decreases with the viscosity of the lower fluid, creating a strong dependence of the flow rate on the viscosity ratio. Due to the balance in shear stress across the interface, a viscosity difference always generates a jump in velocity gradient at the interface. When the permittivities are different, the maximum velocity occurs in the fluid with higher permittivity, as seen in Fig. 2b. It is noted here that the velocity gradient stays continuous across the interface.

In Fig. 3, velocity profiles and corresponding potential distributions are shown for four different values of the interfacial zeta potential jump Z_D when fluid viscosities and permittivities are identical ($\mu_r = 1$ and $\epsilon_r = 1$) and the jump in interface charge density is absent ($Q = 0$). Since the wall zeta potentials are identical ($Z_R = 1$), the potential distribution shows a symmetric profile for $Z_D = 0$. If $Z_D < 0$ ($Z_D > 0$), the potential φ of the top fluid attains more

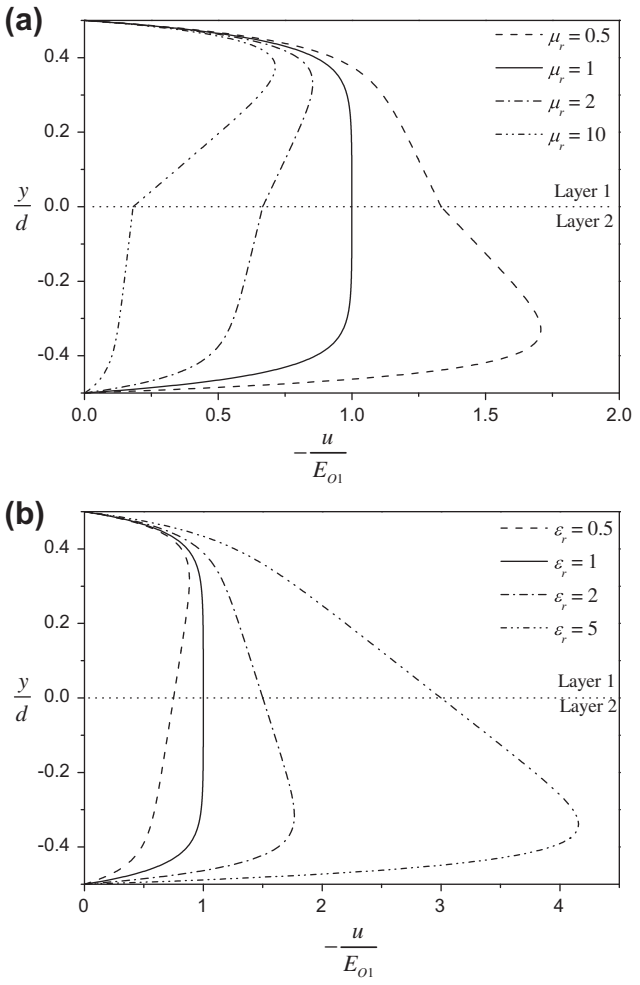

Fig. 2. Velocity profiles for $Z_D = 0$ and $Q = 0$: (a) viscosity variation; (b) permittivity variation.

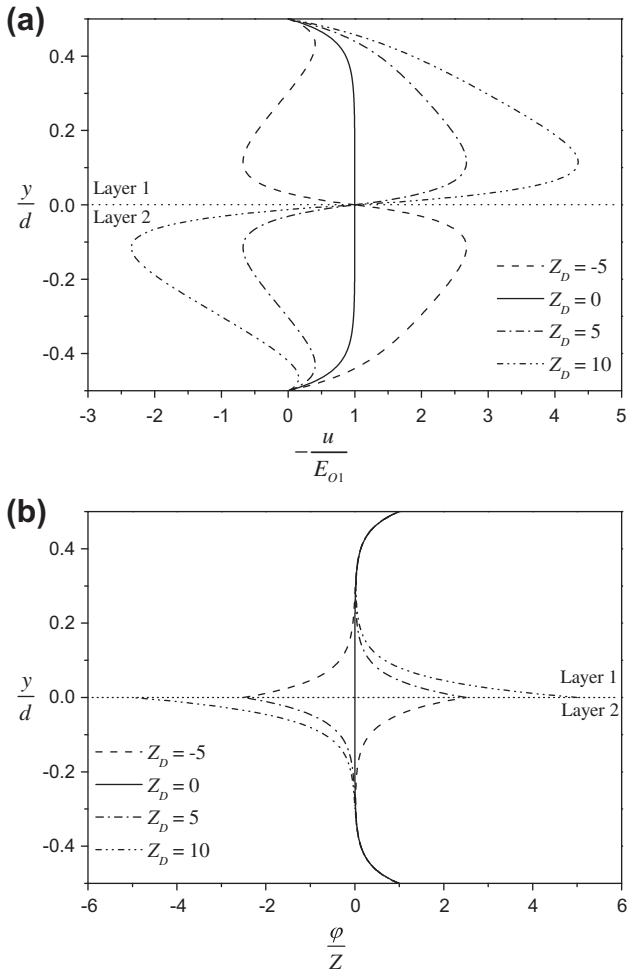

Fig. 3. Velocity profiles and potential distributions depending on interfacial potential jump when $\mu_r = 1$, $\epsilon_r = 1$, and $Q = 0$: (a) velocity profile; (b) potential distribution.

positive (negative) values toward the interface, considering $Z < 0$ for the flow to the right, as shown. The top (bottom) fluid thus tends to be attracted toward the anode, or to the left in Fig. 3, near the interface via electrostatic interaction. Since the interfacial velocities are always identical, due to the no-slip condition (Eq. (12)) imposed on the interface, velocity profiles shown in Fig. 3a are exhibited. For a sufficiently large Z_D, flow reversal can occur due to the electrostatics of the interface, as can be clearly seen in Fig. 3a. It is interesting to note that the interfacial velocity is identical regardless of Z_D. This can be easily understood by examining the interfacial velocity $u(0)$ from either Eq. (14) or (15),

$$u(0) = -\frac{E_{O1}}{\mu_r h_1 + h_2}\left[h_2 + \epsilon_r Z_R h_1 - \frac{De_r}{De_r + \epsilon_r}\left\{\epsilon_r Z_D\left(\frac{h_2}{De_r} - h_1\right) + (\epsilon_r h_1 + h_2)\frac{Q \cdot De_1}{Z_1}\right\}\right], \quad (17)$$

where it is seen that the dependence on Z_D vanishes if $h_1 = h_2$ and $De_1 = De_2$.

In Fig. 4, the jump in interfacial charge density is switched on, while the zeta potential jump $Z_D = 0$ is imposed with $\epsilon_r = 1$ and $\mu_r = 1$. The dimensional surface-charge density $q_s \approx 0.015\ \mathrm{C/m^2}$ when the multiple of nondimensional parameters, QDe_1/Z_1 or QDe/Z for short, chosen here to represent the interfacial charge-density jump, is set to unity with 20 mV zeta potential between the water and the channel wall and Debye length $\lambda_d = 1$ nm. Samec

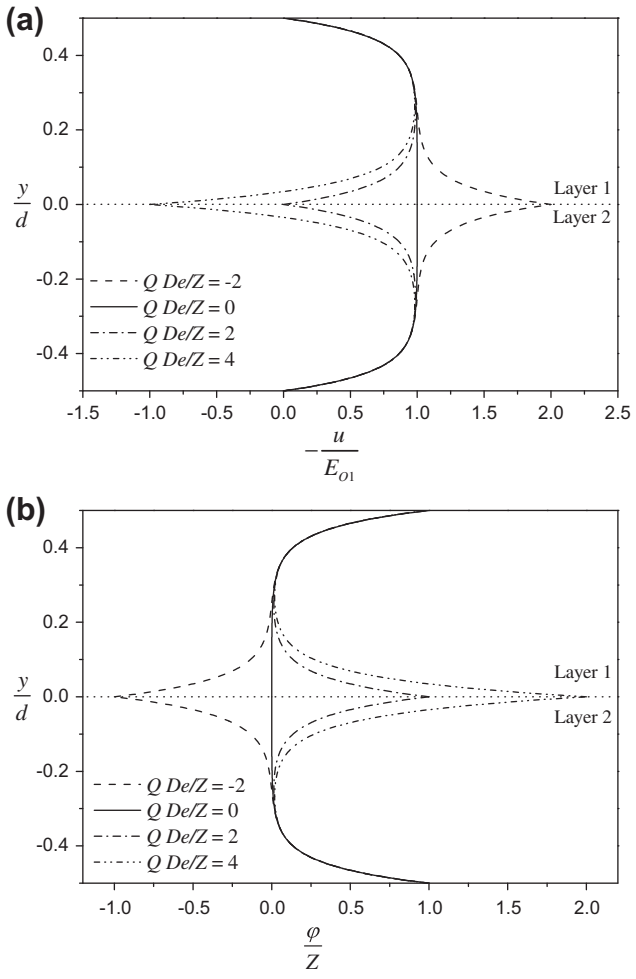

Fig. 4. Velocity profiles and potential distributions depending on interfacial charge-density jump for $\epsilon_r = 1$, $\mu_r = 1$, and $Z_D = 0$.

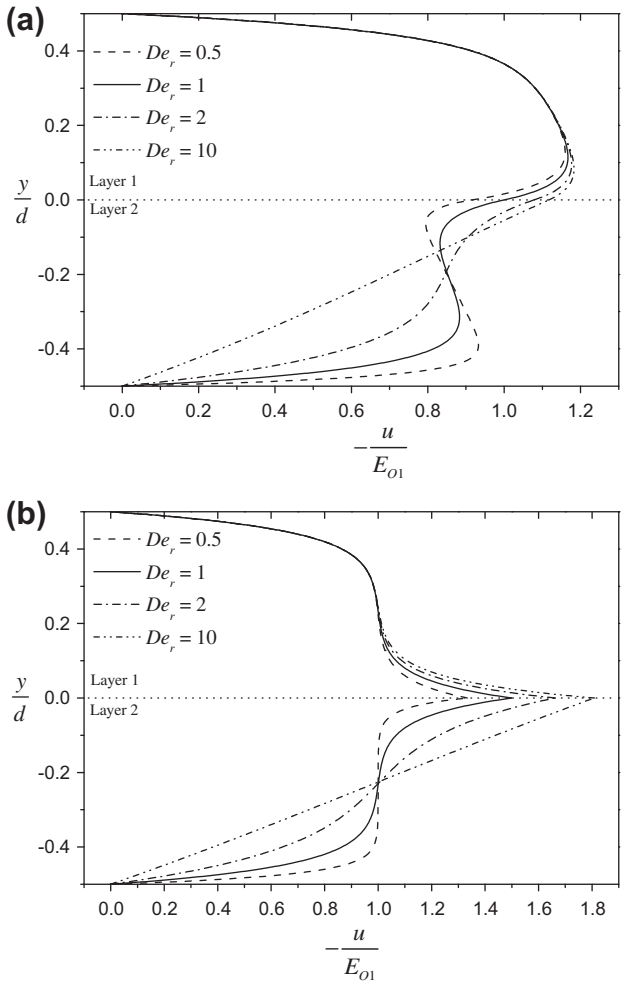

Fig. 5. Velocity profiles for various De_r when $\mu_r = 1$, $\epsilon_r = 1$, and $De_1 = 0.05$: (a) with zeta potential difference ($Z_D = 0.5$); (b) with surface charge density ($QDe_1/Z_1 = -0.5$).

et al. [18] showed that the surface charge density on the water/nitrobenzene interface at various concentrations is in the range of a few tens of millicolumbs per square meter. The parameters chosen in Fig. 4 are thus within reasonable ranges. Unlike the zeta-potential jump, the charge-density jump, does not create additional asymmetry about the interface. With the difference in viscosities and permittivities absent, both the potential distribution and the velocity show symmetric profiles. In contrast to the case with an interfacial potential jump, excess ions with like polarity are accumulated adjacent to the interface on both sides. If $QDe/Z < 0$ ($QDe/Z > 0$), this creates conspicuous flow enhancement (retardation) near the interface, as shown in Fig. 4a. It is seen that the flow retardation can generate a reverse flow along the center of the channel to the opposite direction of the flow near the top and bottom wall.

In Fig. 5, velocity profiles are shown for four different value of Debye length in layer 2 (De_2), while the fluid viscosities, permittivities, and Debye length of layer 1 are fixed as $\mu_r = 1$, $\epsilon_r = 1$, and $De_1 = 0.05$. Higher values of De represent lower conductivities, and so the dynamics in layer 2 become more passive to layer 1. The corresponding velocity field in layer 2 thus approach a simplistic linear profile with the increase in De_2. When the Debye lengths of two layers are different, the magnitude of the electrical potential gradients across the interface are different because the potential would vary with a higher gradient in the thinner Debye layer. Symmetry or antisymmetry in electrical potential, as illustrated in Fig. 3b, thus is no longer maintained. When the potential-jump condition is imposed at the interface, the flow rate seems to decrease monotonically with the increase in De_2. When a jump in surface charge is imposed, however, the flow enhancement, shown in Fig. 4, promotes flow near the interface. The flow rate thus is not diminished as clearly as in the other case.

One of the more useful applications of two-fluid electroosmotic flow is electroosmotic pumping, where a nonconducting fluid can be dragged by an electroosmotically mobile fluid. The behavior of a nonconducting fluid 2 (without lose of generality) can be recovered by imposing lack of ions ($De_2 \to \infty$) and no zeta potential on the bottom wall ($Z_R \to 0$), while maintaining a small Debye-length-to-layer-thickness ratio for fluid 1 ($De_1 \ll 1$). In these limits, the velocity profile (15) of the lower fluid can be simplified, using $\sinh(h_2/De_2) \approx \tanh(h_2/De_2) \approx h_2/De_2$, $\operatorname{csch}(h_1/De_1) \approx 0$, and $\coth(h_1/De_1) \approx 1$:

$$-\frac{u_2(y)}{E_{O1}} = \frac{1}{\mu_r h_1 + h_2}\left[1 + \epsilon_r\left(\frac{h_1 - De_1}{h_2}\right)Z_D - \left(1 + \epsilon_r\frac{h_1}{h_2}\right)\frac{Q\cdot De_1}{Z_1}\right](y + h_2). \tag{18}$$

It is noted that the velocity profile in the nonconducting fluid becomes essentially linear in y. The pumping rate of the lower layer, or the volumetric flow rate, then is simply 1/4 of the interfacial velocity $u_2(0)$, obtained easily from (Eq. (18)). If the top wall zeta potential is negative ($Z_1 < 0$ and $E_{O1} < 0$), the top-layer flow in the absence of any interfacial electrostatics will be away from

the anode, or to the right. This flow can be augmented by the interaction of the imposed external field and excess ions near the interface, quantified by the potential jump Z_D and the charge-density jump Q. It can be deduced from (Eq. (18)) that positive Z_D and Q both enhance the flow to the right, and vice versa. Since for nonconductive media ϵ_r is usually small, the sensitivity to Z_D is expected to be much less than that to Q.

In Fig. 6, $Q\mathrm{De}_1/Z_1$ is thus chosen to be the parameter in showing the velocity and potential profiles of two-layer electroosmosis with a nonconducting layer. The solid line shows a typical profile for electroosmotic pumping in the absence of interfacial electrostatics. No jump in velocity gradient is seen, because $\mu_r = 1$. The case for positive Q corresponds to the broken line ($Q\mathrm{De}_1/Z_1 = -1$) because $Z_1 < 0$ and $E_{O1} < 0$ for electroosmotic flow to the right in Fig. 6. In this case the potential distribution indicates top-layer flow to the right adjacent to the top wall and to the left adjacent to the interface, resulting in the wiggly profile shown. Interfacial velocity is enhanced, as explained above. Overall the flow rate of the conducting layer is diminished, while that of the nonconducting layer is enhanced, which may be desirable in electroosmotic pumping. If $Q < 0$, however, it is seen that the flow of the nonconducting layer can be in the reverse direction at the expense of an enhanced flow rate of the conducting layer. In simplistic electroosmotic pumping this case may be disastrous, but the flow reversal can be useful for a carefully designed microfluidic device. For effective pumping of a nonconducting fluid in the same direction as the conducting medium,

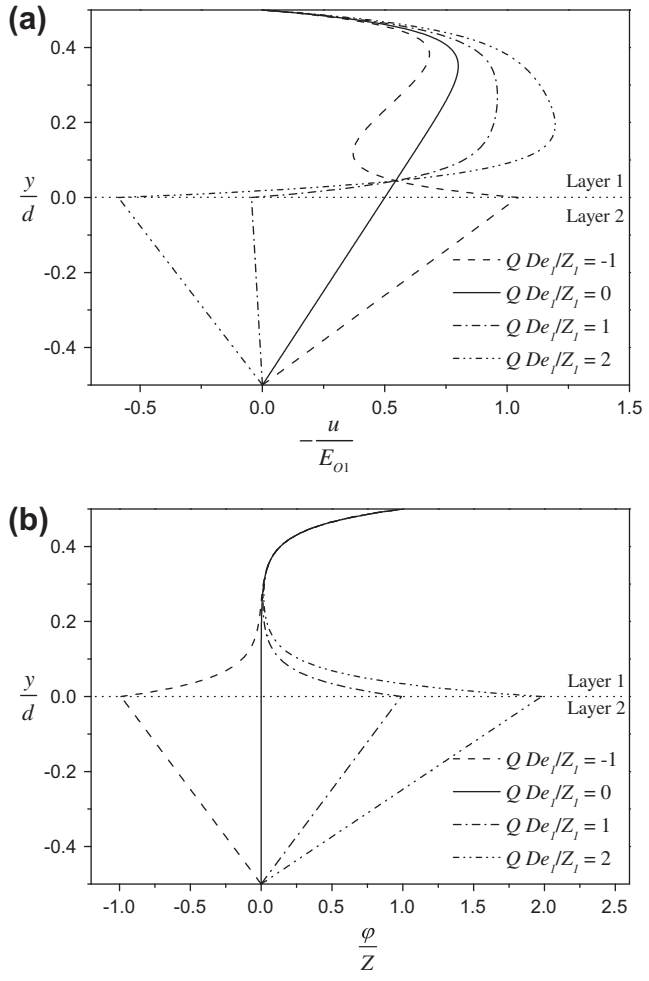

Fig. 6. Velocity profiles and potential distributions in two-layer electroosmosis with a nonconducting lower layer when $\epsilon_r = 0.1$, $\mu_r = 1$, $Z_D = 0$.

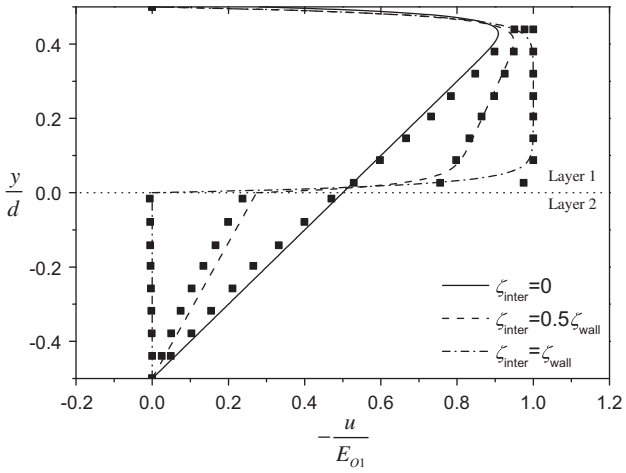

Fig. 7. Velocity profiles obtained by Gao et al. [15] against the present two-dimensional result for three different interfacial electric potential for De = 0.015, $v_r = 1.5$, $Z_D = 0$, and $\mu_r = 1$. $Q\mathrm{De}_1/Z_1$ values varied to match the interfacial potential in Fig. 5 of Gao et al. [15]. Symbol: Gao et al. Lines: present two-dimensional result.

$$\frac{\mathrm{De}_1}{Z_1} Q < 1 \tag{19}$$

must be met.

In actual microchannel flows side walls exist, and three-dimensional effects may have to be considered. Through comparisons with the limited data available in the literature, we suspect that the side-wall effects are localized, and the essential dynamics of the electroosmotic flow is adequately described by the present two-dimensional analysis. As an example, steady-state velocity profiles along the vertical midplane of a rectangular microchannel obtained by Gao et al. [15], who analyzed three-dimensional transient behavior of two-layer (conducting/nonconducting) electroosmosis with a simple interfacial boundary condition of prescribed zeta potential, are compared with the present results in Fig. 7. In matching the prescribed interfacial potential in the analysis of Gao et al. [15] the potential jump Z_D at the interface is set to zero, and the jump Q in charge density is varied. The velocity profiles for three different interfacial zeta potentials in the conducting layer (Layer 1) and the linear profiles in the nonconducting layer (Layer 2) all show good agreements between two- and three-dimensional analysis. The intriguing flow dynamics described above using a two-dimensional analysis thus should exist in actual microchannel flows.

4. Concluding remarks

The zeta potential and the charge density across the interface of two fluids are shown to influence the dynamics of two-fluid electroosmotic flows greatly. Flow reversal due to the electrostatic interaction of the interface with the external field imposed can occur in practical ranges of flow parameters. The flow can also be multiply laminated by fluid motions in opposing directions. The nonconducting fluid in two-fluid electroosmotic pumping assumes a linear velocity profile, and can be clogged or flow in an unintended direction. A careful selection of the conducting medium and flow conditions are thus required, as shown quantitatively in the present study.

For the unidirectional flow studied here, the interface is assumed to stay planar. For practical purposes, the stability of the various flows obtained above needs to be analyzed by allowing the deformation of the interface, which is a good subject for future studies.

Acknowledgments

This work is supported by World Class University Grant KRF R32-2008-000-20082-0 of the Ministry of Education, Science and Technology of Korea. WSC of Potech is also sponsored by the WCU Nano Research Center of Yeungnam University through this grant.

References

[1] A. Brask, G. Goranović, H. Bruus, Technol. Proc. Nanotechnol. 1 (2003) 190.
[2] M. Watanabe, H. Shirai, T. Hirai, Sens. Actuat. B 94 (2003) 267.
[3] V.S. Markin, A.G. Volkov, Adv. Colloid Interface Sci. 31 (1990) 111.
[4] A.G. Volkov, D.W. Deamer, D.L. Tanelian, V.S. Markin, Prog. Surf. Sci. 53 (1996) 1.
[5] J.R. Melcher, G.I. Taylor, Annu. Rev. Fluid Mech. 1 (1969) 111.
[6] D.A. Saville, Annu. Rev. Fluid Mech. 29 (1997) 27.
[7] C.L. Burcham, D.A. Saville, J. Fluid Mech. 452 (2002) 163.
[8] J. Silver, Z. Mi, K. Takamoto, P. Bungay, J. Brown, A. Powell, J. Colloid Interface Sci. 219 (1999) 81.
[9] G. Supeene, C.T. Koch, S. Bhattacharjee, J. Colloid Interface Sci. 318 (2008) 463.
[10] R. Verma, A. Sharma, K. Kargupta, J. Bhaumik, Langmuir 21 (2005) 3710.
[11] V. Shankar, A. Sharma, J. Colloid Interface Sci. 274 (2004) 294.
[12] W. Choi, A. Sharma, S. Qian, G. Lim, S.W. Joo, J. Colloid Interface Sci. 347 (2010) 153.
[13] Y. Gao, T.N. Wong, C. Yang, K.T. Ooi, J. Colloid Interface Sci. 284 (2005) 306.
[14] G.D. Ngoma, F. Erchiqui, J. Micromech. Microeng. 16 (2006) 83.
[15] Y. Gao, T.N. Wong, C. Yang, K.T. Ooi, Colloids Surf. A 266 (2005) 117.
[16] Y. Gao, C. Wang, T.N. Wong, C. Yang, N.T. Nguyen, K.T. Ooi, J. Micromech. Microeng. 17 (2007) 358.
[17] M. Liu, Y. Liu, Q. Guo, J. Yang, J. Electroanal. Chem. 636 (2009) 86.
[18] Z. Samec, V. Mareček, D. Homolka, J. Electroanal. Chem. 187 (1985) 31.